Satellite observations for the geosphere–biosphere programme

Pranav S. Desai* and George Joseph

Space Applications Centre, Jodhpur Tekra, SAC PO, Ahmedabad 380 015, India

This article reviews the role of satellite observations *vis-à-vis* the requirements of the geosphere–biosphere-programme (GBP). An introductory background on the GBP is followed by an analysis of the accuracy requirements for various important parameters classified as those from atmosphere, land and ocean/cryosphere. Satellite sensors addressing some of the observational requirements are discussed, again parameter/theme-wise. In each case, a mention of the principle or approach to the observation is made, and the expected accuracy compared with the desirable one. It is seen that in most cases, sensors are ready to meet the desired level of accuracy, whereas in some cases, such as ocean salinity, near-surface humidity, etc. even the foreseeable state-of-the-art may not be fully adequate, or may have to undergo tests and validation.

THE earth's geosphere – inclusive of land, ocean, atmosphere, cryosphere – has evolved in a way that has made it hospitable for the present forms of life – the biosphere. The biosphere, in turn, plays an important role in the geosphere, in particular in the composition of the atmosphere. Stability of the chemical composition of the environment is maintained by the closed cycles of biospheric substances[1], and there are also other roles of the biosphere (vegetation) in albedo and evapotranspiration. To elaborate on the above, we must take note of the following circumstances:

A simple radiative-balance calculation shows that without the atmosphere, the earth's surface temperature would have been –18°C instead of the actual +15°C; the atmosphere provides a 'warm blanket' via the greenhouse effect of optically active gases, mainly water vapour, carbon dioxide, ozone, methane, etc. The term 'greenhouse effect' refers to the relative transparency of the atmosphere to solar short-wave radiation and the absorption (and re-radiation) of terrestrial long-wave radiation by these atmospheric gases. The downward long-wave radiation provides the extra warming. Figure 1 shows the disposition of absorbed solar energy[2]. Further, water exists in all three phases in the earth system, which also facilitates life forms as found on the earth. The carbon content in the atmosphere – in carbon dioxide, methane, etc. – is actually in a state of dynamic equilibrium; there are large fluxes from and into the biosphere via decomposition and photosynthesis respectively. Until human interference started with the agro-industrial revolution, this balance was maintained[3]. Vegetative cover (as opposed to bare soil) has a lower albedo, resulting in greater absorption of solar short-wave energy – it is theorized that net negative radiative balance created by large-scale depletion of vegetation can cause subsidence and dry conditions (desertification). Vegetation also 'supplies' moisture to the overlying atmosphere via evapotranspiration. It also acts to stabilize the soil against erosion and water against run-off. Needless to add, within the biosphere there are two major classes – plant life and animal life (humans are included in the latter). Oxygen given out by plants during photosynthesis and carbon dioxide from plant/animal respiration, mutually feed these two classes. Global change encompasses changes in climate, terrestrial and marine ecosystems, ocean circulation and sea-level cryosphere and hyrological cycle; these elements are in mutual interplay, particularly at 'climate' time scales of the order of decades to centuries. The processes involved are physical, chemical and biological.

The atmosphere and the oceans interact mainly via the exchange of momentum, heat (latent and sensible), radiation and material such as carbon dioxide, sulphur, etc. The momentum from the atmosphere drives much of the ocean circulation, whereas the moisture/heat input from the ocean is vital for atmospheric dynamics and precipitation. The oceanic biology – phytoplankton fixing carbon dioxide – helps in reducing a part of the atmospheric CO_2 load; the rate of fixation in turn, being nutrient-limited, is largely governed by the upwelling caused by atmospheric forcing/and partly by iron-rich dust. As in the case of marine biological productivity, terrestrial productivity is a significant sink of atmospheric carbon dioxide. In fact, any increase in CO_2 concentration of the atmosphere should accelerate photosynthesis, and this can act as a self-regulator (with negative feedback) within limits – if the temperature is high, then respiration may also increase (CO_2 emission). Further, decomposing vegetation is also a CO_2 source. A complete carbon cycle model will have to include the role of biological processes, such as photosynthesis, respiration, and allocation of fixed carbon among easily decayed components (starch/sugar) vs stable ones (wood, lignin, cellulose, etc.), which in turn are controlled by nitrogen availabi-

*For correspondence. (e-mail: p_sdesai@yahoo.com)

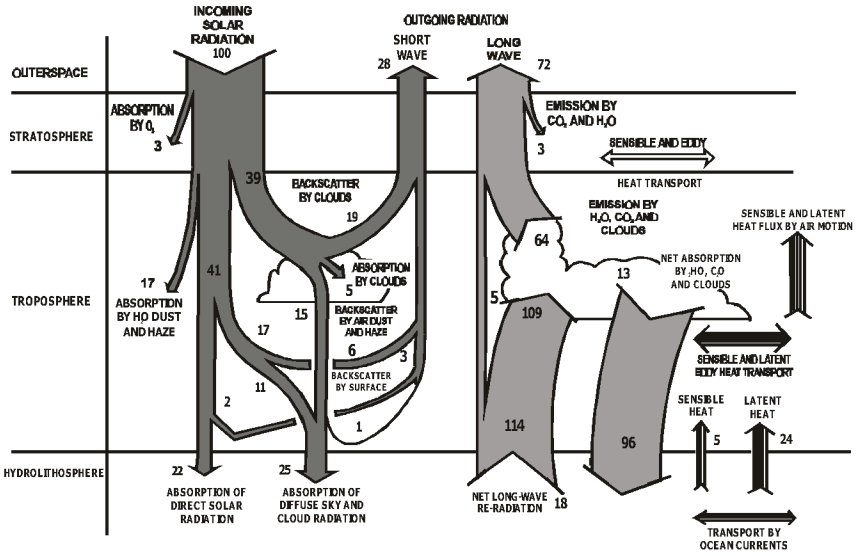

Figure 1. Disposition of solar energy in the earth system. Incoming solar radiation is mainly in the short-wave range up to about 4 μ, whereas outgoing terrestrial radiation is mainly in the long-wave range, beyond 4 μ. Here the numbers are shown with reference to a basic solar input of '100 units'. Clouds, haze and surface play a role (in decreasing order of importance) in reflecting back to space, some of the solar short-wave radiation (28 units). The remaining 72 units are absorbed by the earth–atmosphere system. The overall balance is maintained by the fact that as a 'warm' body, the earth emits its own radiation; the outgoing long-wave radiation is exactly 72 units as seen at the top right section of the figure. However, this is at the 'top' of the atmosphere. At the earth's surface the temperature is much warmer, such that 114 units are radiated. This is made possible by the 'blanketing' effect of greenhouse agents like water vapour, carbon dioxide, clouds, methane, etc. which absorb the long-wave radiation and then re-emit both ways, downward as well as upward. Thus the space mainly 'sees' the earth at a relative cooler cloud level and gets only 72 units, even though the earth is much warmer near the surface, emitting 114 units, because of the intervening role played by greenhouse agents. (Source: NASA[2]).

lity, i.e. the carbon cycle is intimately linked to the nitrogen cycle[4]. The timescales of these biophysical and biogeo-chemical interactions between the land and atmosphere are of the order of a year and a decade respectively, whereas the effect of climate on terrestrial ecology (community composition/large-scale vegetative zones) occurs at even longer scales, i.e. century/millennium[5]. Land-based snow/ice (mountains, polar ice caps) interact with the atmosphere via albedo, heat exchange, etc. Shrinking/melting of glaciers due to atmospheric warming modifies the net albedo and also affects the hydrological cycle. A particular agent of climate change, viz. volcanism is a land-based process. It injects aerosols, gases and heat into the atmosphere, besides causing some local combustion. Sulphate rising to the stratosphere causes radiative changes.

It was Arrhenius[6] who first calculated the effect of doubling of carbon dioxide, which he expected due to the industrial revolution, on the global average surface temperature – he got an increase of about 5°C, not much different from subsequent detailed calculations. The build-up of CO_2, despite oceanic sink, was pointed out by Revelle and Suess[7]. The specific problem of warming due to increasing carbon dioxide from the burning of fossil fuels was addressed first by Callendar[8]. The term greenhouse gas, (greenhouse is a glass enclosure for keeping plants warm in winter), arose from a discussion of the warming effect of such gases. The pre-industrial level of CO_2 is known to be 280 ppmv. The actual record of CO_2 at the observatory in Mauna Loa, Hawaii, USA did show an increasing trend (from 315 ppmv in 1960 to 340 ppmv by 1985; now it is already 360 ppmv). This trend, coupled with preliminary calculations of the carbon cycle, did convince the scientific community that the addition of this greenhouse gas by human action is real and significant. Figure 2 indicates the significance of human perturbation to the carbon cycle[2]. Further, a few other greenhouse gases (like methane) were also expected to add to the enhanced greenhouse warming. Large-scale deforestation and land-use changes were already known to lead to reduced photosynthetic sink for carbon dioxide. Secondly, frictional, albedo and evapotranspiration effect of forests were considered beneficial to climate, and model calculations showed weakening of rainfall in a 'thought experiment' on deforestation[9]. Thus, considering the clearing of forests (for agriculture, pasture, urbanization, etc.) and the burning practices already under way, this too was taken up as an important issue under IGBP.

A significant reduction in the stratospheric ozone concentration was discovered in 1985. Since ozone is known to be a protective shield against solar ultraviolet radia-

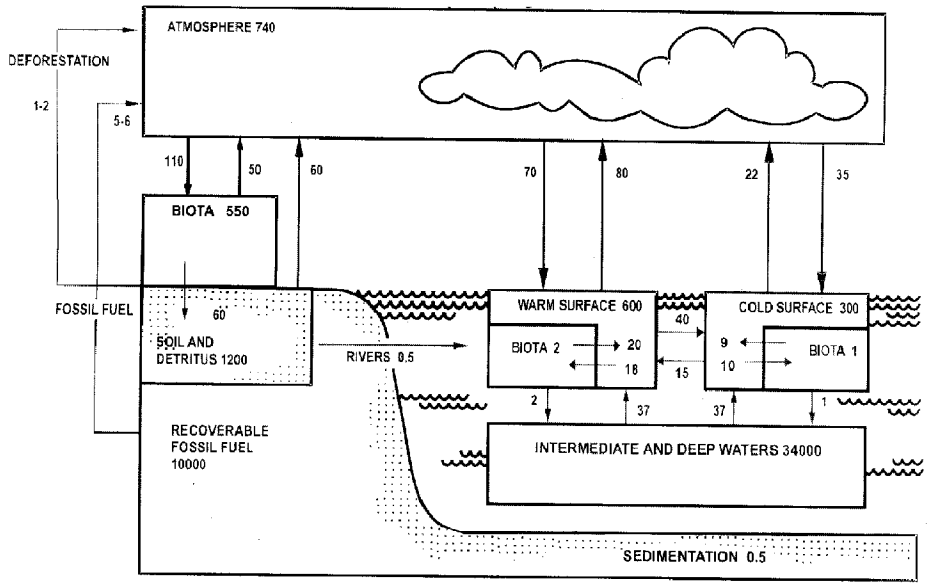

Figure 2. Carbon pools and cycle, and human perturbation in the cycle. Units are 10^{15} g carbon (gc) for reservoirs, 10^{15} gc/yr for fluxes. The carbon cycle has large natural components and fluxes among them, which are in balance. However, by burning fossil fuel, man is accelerating an exchange from a deep dormant reservoir into the atmosphere. Further, forests which are acting as carbon sinks by photosynthesis, when cut or burnt, contribute indirectly by reduced photosynthesis, towards an increase in atmospheric carbon. These two channels shown at the left edge of the panel are significant perturbations to the carbon cycle. (Source: NASA[2]).

tion, this was considered an alarming situation. Analysis traced the problem to increased chlorine (and its family) due notably to refrigeration, which used the inert chlorofluorocarbon in its compressors. The initial observation from an Antarctic ground station was later confirmed by satellite data (Nimbus-7 TOMS). Thus, ozone depletion was also added as a separate problem in International Geosphere Biosphere Programme (IGBP).

Since IGBP requires global as well as repeated long-term observations, satellite-based data collection is an important component. This will be supported by field and laboratory studies. Though IGBP is a highly interdisciplinary programme and requires integration of data from total earth system, we will review the earth observation system, its potential and limitation under three broad areas, viz. atmosphere, land and ocean.

The atmosphere

The data requirement comprises greenhouse gas (GHG) concentrations, including ozone and its predators and precursors due to their global-warming potential[10], and other minor constituents of importance to understand the atmospheric chemistry, aerosol – its distribution and properties, temperature/humidity profiles. The effort is to generate high-quality, long-term data-sets to understand and characterize both anthropogenic and natural changes. Monitoring of ozone was considered important even before satellite-borne instruments were developed and ozone measurements were obtained via ground-based Dobson spectrometer stations. However, obviously it had limited global coverage.

The difference in global mean temperature between the last ice age and the present, is only of the order of 3 K. The corresponding radiation fluxes differ by 4% (from the fourth-power relation). Even the average scenario of global (additional) warming by doubling of carbon dioxide is expected to be around 3 K (after allowing for some compensation by aerosol cooling). The downward infrared flux has increased by 1% (from 300 to 303 W/m^2) since 1900. Thus we are looking for a tropospheric warming and stratospheric cooling – the unique combination 'signature' of greenhouse effect – of the order of 3 K in perhaps 75 years, depending on the assumed rate of emission of carbon dioxide and other greenhouse gases like methane. To observe this trend in a reasonable period of say 25 years (i.e. 1 K/25 years) we seek precision far better than 1 K, say of the order of 0.2–0.3 K. The data processing will have to detect the trend of 1 K/25 years amidst much larger inter-annual/seasonal variability. There will be error-reduction in the process of averaging and curve-fitting; still the basic precision of 0.2–0.3 K is desirable.

Table 1. Concentrations and rates of rise of greenhouse gases

Gas	Concentration (1990)	Rate of increase in concentration (per year)
Carbon dioxide	353 ppmv	1.8 ppmv (0.5%)
Methane	1.72 ppmv	0.015 ppmv (0.9%)
CFC-11 and 12	765 pptv	27 pptv (3.5%)
Nitrous oxide	310 ppbv	0.8 ppbv (0.25%)

The present concentration and observed trends of increase in concentration of GHG gases are given in Table 1 (ref. 11).

As can be seen, the concentrations of methane and carbon dioxide are small, that of nitrous oxide very small, and CFC extremely small (its inert nature gives it a high future potential). All the gases have trends of the order of a per cent per year. Thus, we must not only detect and measure these small levels of concentrations, but also achieve sufficient precision to detect say, in 20 years, changes of 5 to 50% in the various gases. Concentration of ozone is 10 ppmv, reducing at 0.1%/year (in the stratosphere), that of carbon monoxide is at 70 ppbv, NO and ClO have only 0.1 ppbv (stratospheric) concentration.

Natural injection of sulphate aerosols from a medium-sized volcanic eruption is of the order of 10 Tg in the stratosphere, which soon encircle the earth in a narrow belt (but widening by diffusion gradually) and have residence times of the order of 2 years; the corresponding visible extinction optical depth is in the range 0.1. Anthropogenic injection of aerosols, (directly or via gas-to-particle conversions from sulphur-dioxide/pollutants) will not be so dramatic, except in specific sites like dense cities/industrial regions. It may have indirect effect via increase in cloud albedo (provision of more condensation nuclei). However, if the wind-blown loose dust/soil in large areas exposed/desertified by human activities like deforestation, biomass burning/clearing, etc. is included as 'anthropogenic aerosol', then the overall (tropospheric) aerosol load has significant human-induced component. Due to the paucity of aerosol load observations – whether *in situ*, ground-based lidar/MWR, or satellite – it is at present difficult to quantify the expected changes in load, and therefore the required precision. The total columnar optical depth at a station, upon the passage of dust-veil of a recent large volcanic explosion (Mt. Pinatubo), had typically increased from a background of 0.2 to a high of 0.4 after 4 months (at 550 nm). However, detailed change/evolution is needed at an interval of say, 0.02 optical depth.

Land

The data requirements include albedo, vegetative cover and classes, soil moisture, snow/ice cover, overall land-use classes and derived biophysical quantities like evapotranspiration, photosynthetic rate, net primary productivity, surface roughness, momentum and sensible, latent heat exchanges. The generally accepted classification accuracy of land mapping is 90%, with 90% confidence. The mapping of land-use/land-cover changes, including deforestation/desertification as well as snow/ice-cover changes/glacier retreat, is required to be done say, once every five years, and a trend over 25 years may have to be established. To begin with, past data from about 1975 to 2000 may have to be processed. The aims are twofold – inventory of existing bio-resources, and detection of change to know the extent of forest-clearing, snow-cover changes, other land-cover changes, etc. Also, if possible a watch on forest-fire events should be kept (each of which may be small in extent, but if they occur in widespread areas as it happened during El-Nino years in Indonesia, Himalaya, etc, they will have significance in the global context).

The ocean/cryosphere

The climate change will manifest over the oceans through several parameters, the most critical being sea surface temperature (SST), sea-level, ocean circulation, sea-ice and in other cryospheric aspects – polar ice cap (edge and topography), glaciers over land, etc. Further, marine biota plays an important role in the carbon cycle. The SST accuracy of 0.25 K is desirable on climate-scale grids. Data to detect a trend of 1 K/25 years are needed. Global warming is expected to result in overall sea-level rise of the order of a metre in say, 100 years or of the order of a cm in a year. But it is not going to be a uniform rise; initial decades may only show around a few mm per year, accelerating in later decades. Thus, ideally, altimetric/tide-gauge detection of say, 10 cm/25 years should be aimed. Topography of ice-shields and sea-ice is amenable to satellite altimeter (ice-mode) observation with present-day precision, e.g. in Greenland (western ablation zone). The sea-ice extent varies to a great extent seasonally (8 to 15 million km^2 in the Northern Hemisphere and 4 to 20 million km^2 in the Southern Hemisphere), that finding a secular trend will need long record and careful data analysis. The spatial resolution required for sea-ice is 10 km and for snow-cover it is several km (say again 10 km). The global thermohaline circulation monitoring will call for ocean salinity to 1 ppt in climate-scale grids globally – but at critical locations (e.g. in the North Atlantic at the Deep Water Formation Zone), finer grids of 50 km are desirable.

Present satellite capability for IGBP

Atmosphere

The launch of the Total Ozone Mapping Spectrometer (TOMS) on-board Nimbus-7 in 1978 paved the way to

generate global information on total column amount of ozone. Nimbus-7 TOMS was followed by Meteor-3/TOMS (Russian) and ADEOS/TOMS (Japanese) and Earth probe/TOMS. Quick TOMS mission to follow will continue daily mapping of the global distribution of the earth's total column of atmospheric ozone. Though TOMS provides information on global distribution of ozone, it does not distinguish between the stratospheric and the tropospheric components. The first dedicated satellite to make measurements on the atmospheric parameters is the Upper Atmospheric Research Satellite (UARS). UARS carried ten scientific instruments making measurements on various parameters such as solar flux, charged particles, stratospheric minor constituents, including GHGs, nitrogen-containing species, wind profile and UARS sensors.

As far as temperature and humidity profile of the atmosphere are concerned, 'meteorological' sounders are nadir-looking and meant mainly for the troposphere. The principle of sounding in wings of absorption bands is used. For climate/GBP, stratospheric temperatures are equally important; for example, a unique signature of CO_2 effect will be stratospheric cooling, simultaneous with tropospheric warming. For this, 'limb' sounders are more useful as they avoid the background noise of large tropospheric variations (including clouds), and obtain a long path-length through the rarefied stratosphere. An early emission sensor in this category was Nimbus-7 SAMS (Stratospheric and Mesospheric temperature profile; Table 2 lists the sounder), which could give temperature profile in the 15–80 km altitude range (bias 2 K, variation 1 K). The tropospheric nadir sounders, by contrast, give 3 K accuracy.

Principle of atmospheric sounding

Atmospheric sounding is a term probably derived from sonar scanning in the ocean, where sound waves are used to detect underwater objects and also properties of the ocean water. In the atmosphere too 'sodars' are used, but on a limited, local scale only. For broader monitoring of atmospheric properties and constituents, electro-magnetic radiation is employed; still the term sounding has persisted in describing the process.

Even ignoring clouds for the moment, there are gases in the atmosphere which have specific absorption bands or lines and also continuous absorption in some cases, all of which modify the spectrum. As can be guessed, one takes advantage of this modification, i.e. absorption in gas-specific bands, to estimate the concentration of the gas. While the total depletion of radiation in the whole band is a measure of the total load of the gas, finding its vertical distribution calls for a more ingenious approach. For this, a passive sensor with several narrow spectral ranges, all of them located within an overall absorption band of a gas, is employed. The measurement in a spectral channel nearest to the band centre will 'see' the atmosphere as most opaque, and hence sense the emission from an upper layer of the atmosphere, whereas a channel farthest from the band centre will find the atmosphere most transparent, and hence will sense the emission from a lower layer of the atmosphere. In mathematical language, the contribution of radiation into the satellite sensor is a convolution of the falling density profile (of the relevant gas) and the rising transmittance profile, resulting in a bell-shaped 'weighting function' whose peak is located at the upper/lower part of the atmosphere for spectral channel nearer/farther from the band centre. Pressure-broadening of the absorption line permits farther channels easily.

As mentioned earlier, the basic principle behind the sounding of the atmosphere depends on the fact that radiance leaving the top of the atmosphere will be a function of the emitting gas and the distribution of temperature throughout the atmosphere[12]. It was first shown by Kaplan[13] that the vertical temperature distribution in the atmosphere can be inferred from the measurements of upwelling emission around the absorption band of a relatively abundant gas in the atmosphere, which has a uniform distribution and does not vary with place and time. Conversely, the composition of a varying atmospheric constituent can be estimated if the temperature profile is

Table 2. Application of UARS instruments

Observation	HRDI	WINDII	CLAES	ISAMS	MLS	HALOE	SUSIM	SOLSTICE	ACRIM	PEM
Winds	x	x								
Temperature	x	x	x	x						
Pressure			x	x	x	x				
Gas species concentration			x	x	x	x				
Solar irradiance							x	x	x	
Energetic particles										x

HRDI, High Resolution Doppler Imager; SUSIM, Solar Ultraviolet Spectral Irradiance Monitor; WINDII, Wind Image Interferometer; SOLSTICE, Solar Stellar Irradiance Comparison Experiment; ISAMS, Improved Stratospheric and Mesospheric Sounder; ACRIM, Active Cavity Radiometer Irradiance Monitor; HALOE, Halogen Occultation Experiment; PEM, Particle Environ Monitor; CLAES, Cryogenic Limb Array Etalon Spectrometer; MLS, Microwave Limb Sounder.
UARS was launched in September 1991.

constant or known. To understand the vertical sounding, consider an arbitrary spectral line shown in Figure 3, which gives transmittance (1-absorption) versus wavelength. By making observations from the top of the atmosphere in a highly absorptive region, as at $\ddot{e}_3$, the instrument (radiometer) will 'see' only a limited distance into the atmosphere. When observations are made at wavelengths close to the transparent edge of the absorption line, as at $\ddot{e}_1$, the radiometer gets a deeper 'look' in to the atmosphere. For observations at wavelengths between the above two, as at $\ddot{e}_2$, the sensor can see regions between the top and bottom of the atmosphere. Thus, if measurements are carried out at a number of wavelengths, the relative contributions from the different heights (more correctly pressures) will vary. In other words, the radiation received has contribution from throughout the atmosphere. The altitude of the peak of the weighting function depends on the absorption coefficient at the particular wavelength. Figure 4 gives the weighting function of a typical space-borne sounder.

For temperature sounding, the emitting constituent should be substantially uniformly mixed in the atmosphere so that the emitted radiation can be considered as a function of temperature distribution only. For temperature sounding of the atmosphere both O_2 and CO_2 satisfy these conditions. CO_2 has two absorption bands at 15 and 4.3 μm, which can be used up to 80 and 35 km, respectively[14]. O_2 absorption band is in the microwave region (5 mm) which can be used up to 100 km. The retrieval of temperature profile from a suitable set of spectral radiances begins with the forward equation essentially relating the vertical temperature distribution in the atmosphere to the intensity of outgoing radiation. For temperature sounding, we have to 'invert' this equation of radiative transfer so as to get temperature as a function of pressure. The details of the technique of inversion are quite involved[15–20] and beyond the scope of this article.

Limb sounding

The geometry we have considered for the above discussion is nadir (or near-nadir) view, wherein radiation is observed leaving the atmosphere along (or close to) the local vertical. An alternate technique to nadir sounding is to view the radiation leaving the atmosphere nearly tangentially, called limb sounding. Limb sounders are passive sensors viewing through a long tangential atmospheric path. These can work in 'emission' mode (dark space background) or 'absorption' mode (bright objects like the sun or any other star as a background, to create 'occultation'). The long path provides increased amount of the trace gas than earth-viewing path, besides avoiding 'clutter' from ground/clouds. The majority of climate-related gases (ozone, etc.) are in the stratosphere. So this is a suitable geometry for them. The star occultation makes the geometry more precise, so the tangent height (and temperature) are better known. However, one limitation of limb sounding is that only 'integral' measurement along the long path is obtained. Several paths at different heights can be combined to infer the vertical profile of the constituent. Aerosols are also measurable using a window channel of 1 μm. The geometry of limb-viewing is shown in Figure 5. The major advantages of limb-viewing are high vertical resolution, black background (emission mode), large opacity and large area coverage. The disadvantages of limb sounding include poor horizontal resolution (~ 500 km) and cloud contamination. Since in the earth's atmosphere clouds are usually in the troposphere, reliable observation using limb sounding is limited to the upper troposphere and above. The alignment uncertainty of the instrument to satellite axis and the satellite attitude error affect the accuracy with which the absolute height can be deduced. By making measurement in two bands – one narrow (630–685 cm^{-1}) and the other broad (585–705 cm^{-1}) of CO_2 absorption band, the height can be derived. This is based on the principle that to a first approximation, the ratio of the signals from the two bands is independent of temperature[21]. Several temperature-retrieval techniques are available[21–23].

Backscatter and absorption techniques for sounding

Till now, we have been considering the retrieval of temperature profiles/constituents by making measurements on their emission bands. This does not require any extraneous source. However, it is possible to sound minor constituents of the atmosphere by observing the scattered solar radiation or from the observation of the absorption of solar (or stellar) radiation. Consider a satellite-borne instrument (in the visible, ultraviolet, near-infrared range) looking down into the sun-lit atmosphere. Using the known cross-section of absorption and scattering and using a standard atmosphere, it is possible to deduce vertical distribution of ozone from the observed backscat-

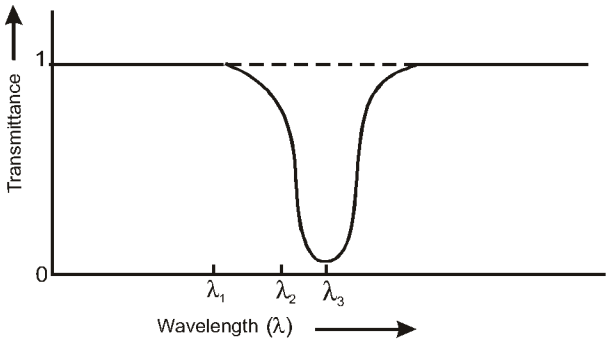

Figure 3. Transmittance vs wavelength: choices for sounding. Here, transmittance is (1-absorption). Wavelengths $\ddot{e}_1$ to $\ddot{e}_3$ illustrate decreasing penetration of a sounder's view into the atmosphere.

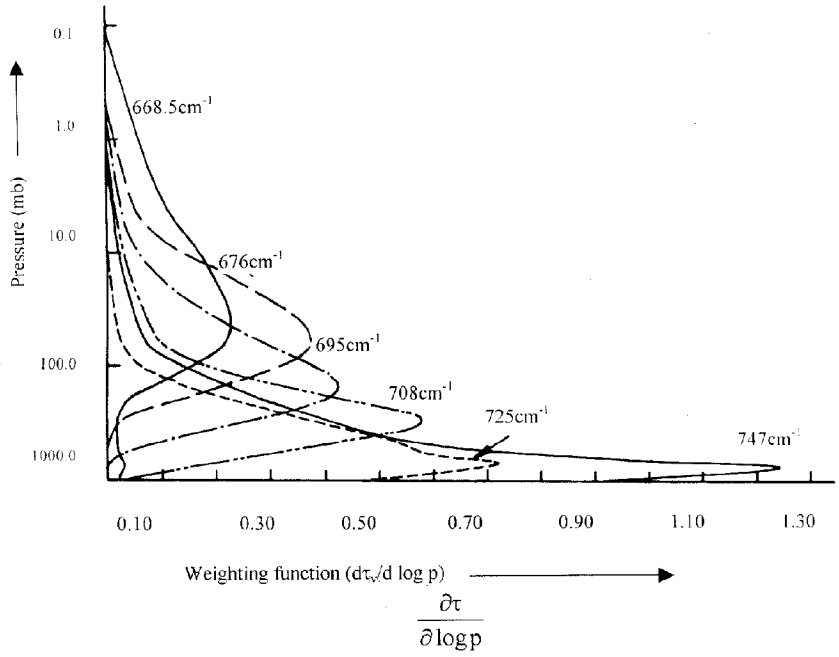

Figure 4. Typical weighting function of a sounder (earth view). 747 and 668.5 cm^{-1} typify $\ddot{e}_1$, $\ddot{e}_3$ in Figure 3.

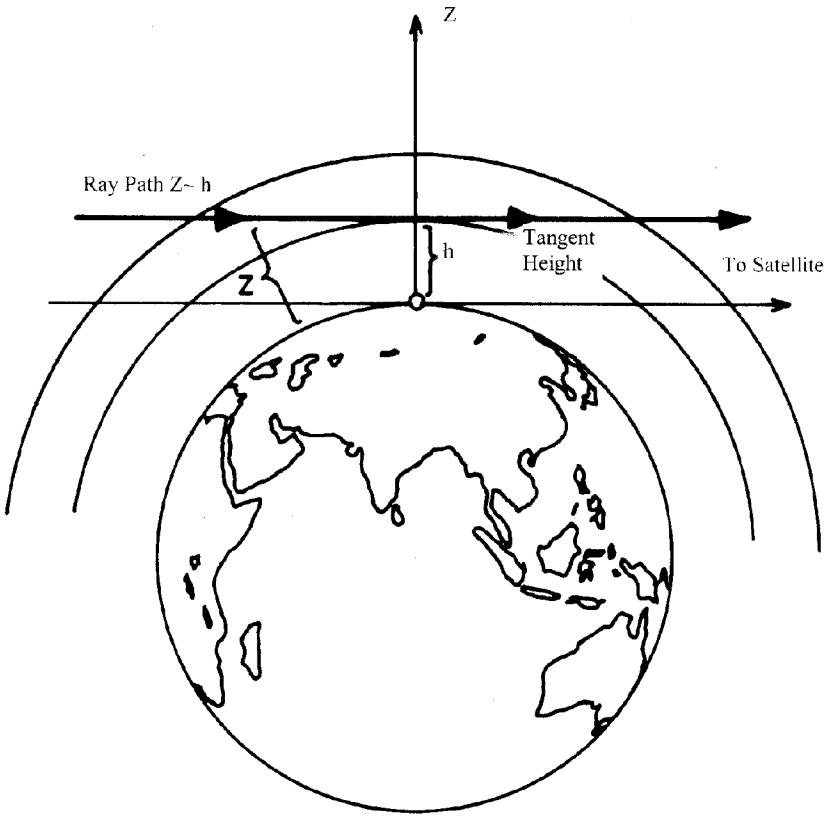

Figure 5. Geometry of limb sounding. The satellite senses radiation from a long path at tangent to height *h*.

tered ultraviolet radiation[24–26]. This principle is used in the solar backscatter ultraviolet (SBUV) and TOMS instruments flown on-board Nimbus satellites[27].

In the occultation technique, classical absorption spectroscopy is used to determine the number density profile of the absorbing species. The sun or star is used as the source of light, the satellite instruments as detectors and the intervening atmosphere as the absorption cell. Measurement at successive satellite positions in the orbit corresponds to rays travelling the atmosphere at different heights, thereby providing the vertical profile of the absorber. The best results are obtained when the absorption bands do not overlap and are well-separated[28–30].

Active sounding of atmosphere: We have been discussing 'passive' sounding of atmosphere, since naturally-occurring radiation (self-emission, sun, stars) was used for probing. Active remote sensing of atmosphere using lasers has been used successfully for obtaining atmospheric parameters. LIDAR is used to probe the atmosphere using laser pulse. The emitted laser pulse interacts with atmospheric constituents and a small fraction of the energy is scattered back to the LIDAR. Study of the intensity variation, changes in the polarization or the frequency shifts of the backscattered radiation can yield information on the physical state (temperature, pressure, wind profile, etc.) and the molecular composition of the atmosphere. The distance to the scattering medium can be deduced from the time delay of return signal, providing excellent vertical resolution. Some of the laser techniques which are of importance in atmospheric probing are backscatter lidar, differential absorption lidar (DIAL), Raman backscatter lidar.

Sensors for atmospheric sounding: The purpose of this section is to give a general outline of the techniques involved in realizing an atmospheric sounding instrument without getting into the engineering details of the instruments. For sounding the atmosphere – either to measure temperature profile or the composition – we have to measure the emission/absorption spectra. For example, to measure the vertical temperature profile, measurements are to be made in a number of narrow spectral bands within the absorption band of CO_2. A generalized block diagram of an atmospheric sounder is given in Figure 6. The instrument essentially consists of a collecting optics which collects the energy in the wavelength region of interest and is followed by a system for spectral selection. The spectral selection could be achieved in the most simple case by a filter wheel or in more advanced systems using an interferometric system. The spectrally-selected radiation falls on suitable detectors. The output of the detector is suitably amplified and further processed for recording or transmission. The major challenge is to realize an instrument with good resolution in the horizontal direction and vertical height with high radiometric sensitivity to derive temperature/gas density of adequate accuracy.

As mentioned earlier high spectral resolution is required for better height resolution, while narrower the spectral band lesser will be the energy collected, resulting in poor temperature (flux density) accuracy. Different innovative techniques have been used to realize instruments to provide best performance. The basic difference in all these instruments is how the spectral selection is realized. However, in the occultation geometry, measurement is carried out in the total absorption spectrum. Some of the commonly used spectral selection techniques are interference filters, prism or grating, interferometry and use of gas cell with modulated pressure[31–36]. Apart from the IR systems described above, microwave sensors are also extensively used to sound the atmosphere for temperature profile and minor species concentration determination[37–40].

Aerosol is a complex constituent to monitor, due to the difficulty and intricacy of retrieving aerosol parameters.

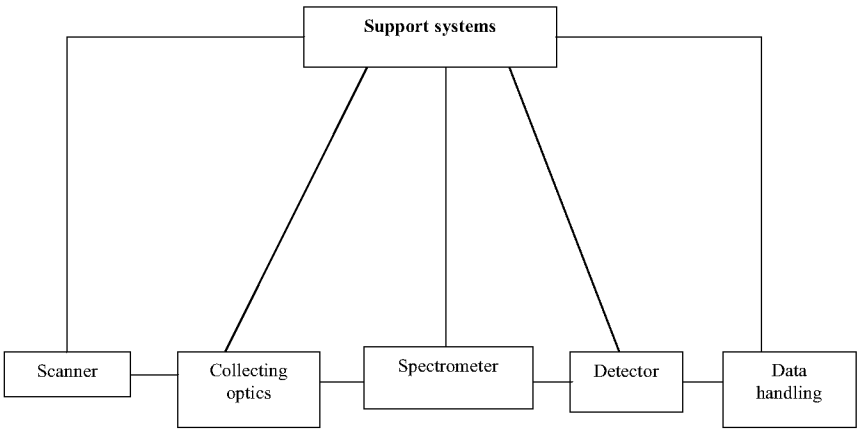

Figure 6. Schematic of atmospheric sounder components.

There have been experimental payloads for aerosol sensing, such as stratospheric aerosol and gas experiment – the first one was on Atmospheric Explorer Mission-2 (February 1979 to November 1981), giving aerosol load to 10% accuracy in 1 km layers from 10 to 25 km, and 20–50% accuracy in 5 km layers from 25 to 40 km. It was a sun occultation photometer in limb view with 1 μ channel for aerosols (and 3 other channels for gases like ozone and NO_2). Another experimental payload is German Multispectral Opto-electronic Scanner (MOS-A) using 750 nm oxygen channels to sense aerosols in two broad layers of the atmosphere, the stratosphere and troposphere – this is placed aboard the Indian Remote Sensing Satellite IRS-P3 launched in March 1996. Attempts are also made to use operational satellites; for example, NOAA–AVHRR channel-1 over the ocean, or the NDVI (Normalized Difference Vegetation Index) over dense forest, to detect aerosol load. The NDVI will register a significant decrease upon passage of volcanic aerosol plume over the forested area, due to the reduced contrast between radiances in channels 1 and 2. Finally, cloud cover is another important atmospheric dataset. The NASA–NOAA pathfinder includes AVHRR cloud map (pathfinder is a long-term, consistently calibrated global change-related dataset from multiple satellites).

Land

Traditionally, land surface classification and mapping are done for earth resource application such as agriculture, forestry, geology, etc. from high-resolution sensors on land-oriented satellites such as US Landsat, Indian Remote sensing satellites. However, for climate-scale applications, averaged properties over much larger domains – typically 100 km – are needed. But the derived quantities mentioned above are nonlinear functions of basic land classes or properties. Still, 30 m would be too fine a resolution to be handled as the data rate and computations will be prohibitive. As a medium solution, 1 km sensors notably NOAA–AVHRR (also GOES–VHRR, INSAT–CCD, IRS–WiFS, etc. of commensurate resolution) are used to map land features and then climate-scale averages of additive quantities are found. The most prevalent quantity from NOAA is the NDVI, which is empirically related to net dry bio-mass. Overall land-use classes are also mapped from NOAA–AVHRR. The NASA–NOAA pathfinder dataset includes (daily 8 km and 10-day composite over 100 km grids) NDVI maps. For soil moisture, there is no operational sensor at present. In arid zones, the thermal inertia as sensed in geo-synchronous VHRR (IR channel) may be related to soil moisture. Microwave radiometers such as Nimbus–SMMR have been used experimentally to sense soil moisture. Snow/ice cover also is amenable to mapping with microwave radiometers, such as Nimbus–SMMR, DMSP–SSM/I, etc. Visible and IR data from Landsat and SPOT have also been used in mapping continental snow cover, but the data rate is too high to be of practical use in climate studies. In general, the higher-resolution earth resource-oriented satellite imagery[41] may be useful at calibration sites to cross-validate the average land features obtained from medium-resolution sensors like NOAA–AVHRR. As far as derived quantities such as photosynthetic rate, evapotranspiration, etc. are concerned, again field-level ecological experiments have to be used to assign quantities to classes of vegetation as seen from satellite data.

Ocean/cryosphere

SSTs (besides those of ships and buoys, i.e. *in situ* data) are observed by satellites, notably NOAA–AVHRR, particularly more accurately after the introduction of split thermal window since NOAA-7 (1981). The NASA–NOAA pathfinder (climatic reprocessed) dataset includes monthly mean SST fields from NOAA–AVHRR since 1981 to date. The basic absolute accuracy of SST from AVHRR is 1.5 K, based on buoy comparisons. The experimental sensor Along Track Scanning Radiometer (ATSR) on ERS-1/2 uses multi-angle approach to atmospheric correction and yields SST to a better accuracy of about 0.5 K. It should be mentioned that such low-orbiting satellites can suffer from bias due to diurnal cycle – even in monthly averages, such additional effects have been estimated to add about 0.3 K error.

Sea-level rise caused by global greenhouse-warming (via ice-shelf dynamics, glacier melting, thermal expansion, etc.) may be around 0.5 cm per year at present – it may increase in future. Thus, at least a 15-year record of satellite altimeter (accuracy typically 5 cm at state-of-the-art instrumentation and processing) is needed to detect the rise. Since high-precision TOPEX altimeter (with dual frequency for ionospheric correction) is only about seven years old, definitive conclusion will have to wait another decade or so. Sea-ice is amenable to microwave remote sensing. Radiometers like Nimbus–SMMR, DMSP–SSM/I and NOAA AMSU-B give sea-ice concentration with 10% accuracy in 50 km grids. Altimeter can give iceberg topography and SAR can give finer details (more useful for navigation than for climate studies). Further, DMSP also has 0.6 km visible imagery – the albedo variation (typically over the Arctic, 0.4 in August, 0.75 in May) is an indicator of ice cover. A good example for the analysis of sea-ice covers for climate-related purpose, from Nimbus–SMMR data (1978–87) is presented by Gloersen and Campbell[42], who found around 0.2% per year decrease as a secular trend in Arctic ice-cover (riding over periodicities). The land-based snow cover (clubbed here under 'cryosphere' although not part of 'oceans') is mapped by NOAA AMSU-B, but at a poor accuracy of 50%. NOAA–AVHRR also can give snow

and ice-cover maps, and so also the Wide-Field Sensor (WiFS) on Indian Remote Sensing satellites, besides the imagery from Landsat and SPOT. Mountain glaciers are among the more sensitive indicators of global warming, and a 13% shrinkage of global mean glacier volume in a century is already detected[43].

Radiation

The special sensor called ERBE was placed for radiation budget on a complex of US satellites, ERBSAT and NOAA 9/10. This has given adequate insight, but the duration of data span was limited. Similarly, a French sensor ScaRaB was placed on the Russian satellite METEOR. The sensor CERES placed on TRMM also measures radiances in the 'total range' (0.2 to 100 μ), short wave (0.2 to 3.5 μ) and long wave (6 to 25 μ).

Long-term monitoring of climate from satellites

A continuous and consistent watch over climate-related parameters on a global scale by a carefully inter-calibrated series of satellites is accepted as a desirable component of climate-change monitoring strategy. In this context, it is natural that a question may arise as to how far the available satellite datasets have been helpful in delineating climate change (if any) since the advent of satellites, roughly about 40 years ago. Here, the evolving nature of satellites and sensors, makes it a complex task to relate successive satellites and develop a consistent long time-series of climatic parameters. The NOAA–NASA pathfinder programme is an effort in this direction, to re-process data from past satellites so as to evolve a consistent dataset for climate studies[42,43]. One of the longest time-series available is that of earth radiation budget components[44] from scanning radiometer of NOAA satellites (and successer sensors), although these being based on narrow bands, are not as accurate as those from specific Earth Radiation Budget Sensors. The same NOAA has been also used to prepare another of the longest time-series, viz. areal coverage of snow on a weekly basis by visual interpretation of imagery from 1966 to date, of which data from the first six years are said to suffer from some underestimates. The data from 1972 to 1992 clearly show a secular decreasing trend of approximately 1% per year, in spring and autumn (only), over the Northern Hemisphere[45]. Unlike the change in solar radiation which will warm or cool the entire atmosphere, increase in GHG traps some more terrestrial warmth in lower layers, thereby warming the troposphere and cooling the stratosphere. Therefore, the best signature of greenhouse effect is a rising lower tropospheric and falling stratospheric temperature[46] as shown in Figure 7; satellites and balloons do show this in 1960–2000. For future monitoring of climate forcing and feedback, Hansen *et al.*[47] have proposed 'climsat', a low-cost series of satellites having SAGE, EOSP and MINT (Michelson interferometer) – complemented by ACRIM on separate satellites, and *in situ* data.

Accuracy and resolution of some recent and forthcoming sensors

Atmosphere

Temperature profile: The optimal scenario will use a combination of infrared and microwave sounders to take care of cloud-free and clouded areas respectively. The recent generation of TOVS (HIRS, MSU, SSU) gives temperature profiles from about 1 km to the stratosphere, with horizontal effective resolution of 50 km and temperature accuracy of 3°C or so. The next generation sounders are listed below, with names of satellites in parentheses:

AIRS (EOS PM-1): Temperature profile at 1 km vertical and 50 km horizontal resolution, with accuracy of 1°C (cloud-free/partly clouded areas). It has high spectral resolution with wavelength-to-bandwidth ratio of 1200, in the range 0.4–15.4 μ, with 3600 channels – the 'clean' super-windows sense the surface, and opaque channels sense the atmosphere.

IASI (METOP): Temperature profile in the troposphere is measured at 1 km vertical and 25 km horizontal resolution with accuracy of 0.5–2°C (interferometer approach). It works in the spectral range 3.4–15.5 μ.

Humidity/moisture profile: The new generation sounders – both infrared such as AIRS, IASI and microwave such as AMSU-B, MHS will provide greater vertical resolution besides all-weather capability in the latter, around 3 km.

SAPHIR (Megha-Tropiques): Cross-track sounder at 183 GHz band (H-pol), with 10 km resolution, inter-channel 0.5 K, giving water-vapour profile in six layers (2–12 km).

AIRS (EOS PM-1): Humidity profiles will be derived from channels in the 6.3 μ and 11 μ band/window.

IASI (METOP): The horizontal resolution is 25 km and the accuracy of specific humidity is 0.1–0.3 g/kg, which in a typical situation amounts to 5%. It works in the spectral range 3.4–15.5 μ.

AMSU-B (NOAA K-M): The horizontal resolution is 15 km (at nadir) with specific humidity profile at 10–20% accuracy.

MHS (NOAA-N, METOP): Provides atmospheric humidity profile at horizontal resolution 30–50 km, vertical resolution 3–7 km, and accuracy of specific humidity profile is 10–20%. Spectral bands are: 89 GHz and 183 GHz – wings (four channels).

MADRAS (Megha-Tropiques): Microwave imager for rain, integrated water vapour, liquid water, ice/cloud tops with channels 19, 24, 37, 89, 157 GHz.

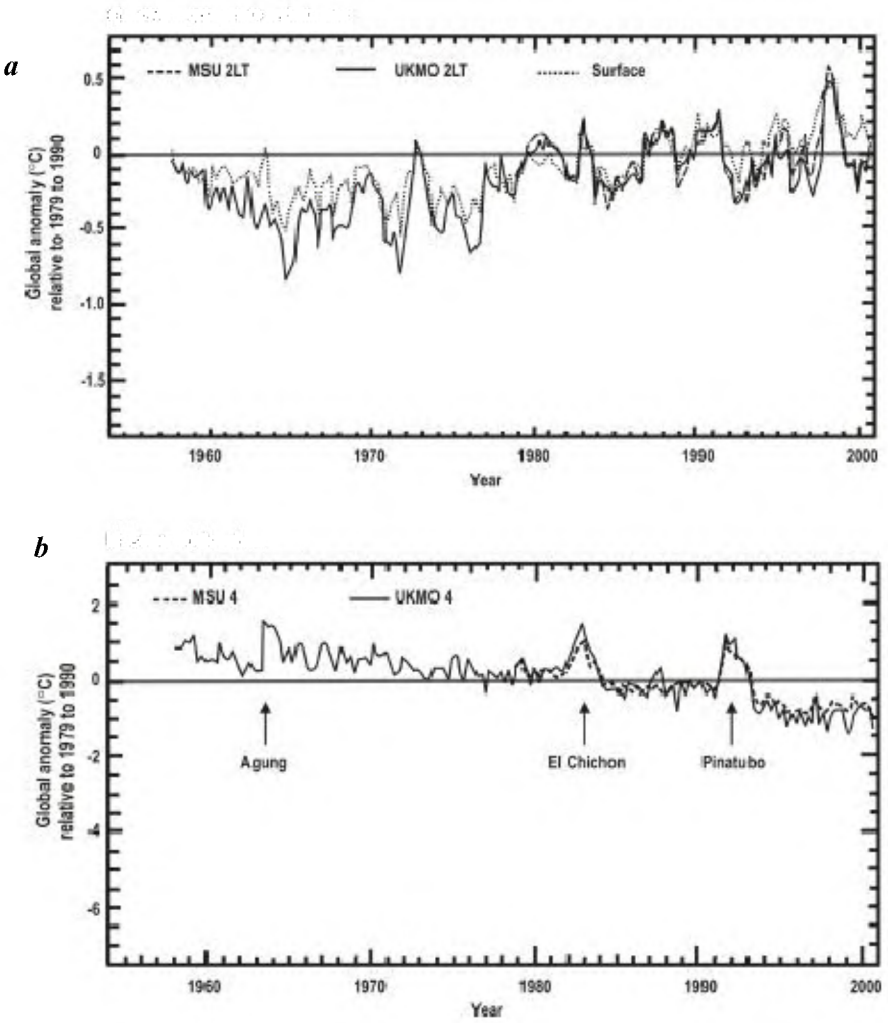

Figure 7. ***a***, Anomalies of global average temperatures 1958–2000 relative to 1979–1990, for the lower troposphere from satellite microwave sounder and balloons (UKMO) and for the surface. One can observe an increasing trend for the lower troposphere and surface. ***b***, Similar to ***a***, for the lower stratosphere. Here, observations from satellite sensor microwave sounder and balloons (UKMO) are shown. A decreasing trend is seen here. The tropospheric warming, simultaneous with stratospheric cooling, is indicative of increasing concentration of greenhouse gases, mainly in the troposphere; they keep some more terrestrial radiation in lower layers. (Source: IPCC 2001 Report adapted from Jones[46].)

Ozone – total column and profile: At present, total ozone is measured by SBUV on alternate NOAA satellites. Ozone profile is measured by GOME on ERS-2 at a 5 km vertical and 40 km × 40–320 km horizontal resolution using differential absorption method. The experimental satellite UARS has four sensors for ozone. Among future sensors, the following are noteworthy:

GOME-2 (METOP): The horizontal resolution will be 160 km, vertical 5 km and the trace gas profile (ozone and its destroyers) at 10–20% accuracy. It works in the band 0.24–0.79 μ.

GOMOS (ENVISAT): This is a self-calibrating, star-targetted sensor with 1 km vertical resolution for ozone (and a few other trace gases). The sensor (typically 25/orbit) will permit 0.05% per year change in ozone to be deduced over its five-year life.

SCIAMACHY (ENVISAT): Provides tropospheric and stratospheric profiles of ozone (and several other trace gases) at horizontal resolution 30 km × 200 km and vertical resolution 2.4 km, with radiometric accuracy of 4%. The total columnar accuracy is expected to be 1%. Also gives polar stratospheric clouds on which Ozone is destroyed. It works at limb in sun and moon occultation modes using differential optical absorption spectroscopy, and also has a nadir mode for total column values of trace gases and aerosols (0.24–2.4 μ).

MIPAS (ENVISAT): While this will have spatial resolution similar to that of SCIAMACHY, the radiomet-

ric precision being 1%, the net ozone accuracy would be better. The vertical range is from 8 to 100 km. It is a high-resolution Fourier transform IR spectrometer in limb emission mode (4.2–14.6 μ).

HIRDLS (EOS CHEM): The trace gas accuracy for ozone (and a few of its destroyers) is 10% in volume of 1 km (vertical) × 10 km (across) × 400 km (along line of sight), in a limb view. (Also detects polar stratospheric clouds where ozone is destroyed). It performs limb scans in the vertical at multiple azimuth angles, measuring IR emissions in 21 channels from 6 to 18 μ.

TES (EOS CHEM): This will be the only sensor to detect ozone even at the surface and upwards to the lower stratosphere. It will give 3D profiles of virtually all IR-active species. It has limb mode at 2.5 km height resolution and a down-looking view at 50 km × 5 km. Ozone accuracy is 20 ppbv. It is a high spectral-resolution IR-imaging Fourier transform spectrometer in the range 2.3 –16.7 μ.

AIRS (EOS PM-1): Total ozone is obtained by the 9.6 μ absorption band. But water-vapour correction will be called for, hence the accuracy may not be high.

IASI (METOP): Total ozone is obtained using 9.6 μ band, with 10% accuracy.

SAGE-III (EOS-AERO AND EOS-CHEM): Profiles of ozone (and other few minor constituents) at 6% accuracy for ozone, at 1 km vertical resolution. It is a limb-scanning grating spectrometer in the waveband 0.29–1.55 μ.

ILAS-II (ADEOS-II): Measures ozone only in high-latitude zone, in the altitude range 10–60 km, at a vertical resolution of 1 km and horizontal resolution of 13 km, with an accuracy of 5%. This uses prism and gratings to detect the absorption spectrum of the earth's limb against solar background in two ranges: 0.75–0.78 μ. 2–13 μ.

MLS-2 (EOS-CHEM/PM): Lower stratospheric concentration of ozone, but only at 50% accuracy, with a resolution of 4 km (vertical) and 10 km (horizontal). It has limb emission measurements at 215, 310, 640 and 2500 GHz.

SAFIRE (proposed): This will provide ozone-related species and processes, besides permitting detection of climate change in the stratosphere. Dynamics/chemistry coupling will be studied.

Aerosols: As mentioned earlier, there is no routine aerosol-monitoring sensor on the current satellites although NOAA–AVHRR and ERS–ATSR, Channels-1 over the oceans, and NDVI over dense forests are used to infer aerosol load approximately. Future sensors are listed below.

ATSR-2 (ERS-2), AATSR (ENVISAT), CCD CAMERA (INSAT-3A), AVHRR/3 (NOAA K-N): Due to the SWIR (1.6 μ) channel, these will give aerosols/volcanic eruptions.

MODIS (EOS-AM/PM): Aerosol load/opacity and properties; opacity accuracy 10%. EOS-AM with MODIS has been launched recently. The spectrometer (nadir/tilt) has 36 spectral bands between 0.4 and 14.5 μ (irradiance accuracy 5% up to 3 μ and 1% beyond 3 μ).

MISR (EOS AM-1): Aerosol load/opacity and properties, opacity accuracy 10%. It provides planetary and surface albedo and aerosol, including angular reflectance functions, with 15 km resolution.

SCIAMACHY (ENVISAT): Provides tropospheric and stratospheric profiles of aerosols.

SAGE-III (EOS-AERO and EOS-CHEM): Profiles of aerosol at 2 km vertical resolution, with 10% accuracy. This is an earth-limb scanning grating spectrometer with self-calibrating solar/lunar occultation in nine channels from 0.29 to 1.55 μ.

GOMOS (ENVISAT): Profiles of aerosols in the stratosphere, with 1 km vertical resolution.

HIRDLS (EOS-CHEM): Measures concentration of aerosols in a volume 1 km × 10 km × 400 km.

ATLID (ESA): Active (lidar) futuristic sensor for aerosol and cloud properties at 1.064 μ with 100 m horizontal resolution as well as 100 m height accuracy. Shot spacing will be of the order of 50 km.

Other trace gases: CFCs, methane, NO_2 are the most important greenhouse gases after carbon dioxide. (Since CO_2 is employed to infer the temperature profile, direct measurement of CO_2 is not envisaged). Ozone has been already covered above. CFCs also have another (adverse) role – they destroy ozone. The UARS sensors for monitoring trace gases are the following:

CLAES (3.5–12.7 μm): Solid, hydrogen-cooled interferometer looking at limb in IR for HNO_3, N_2O, O_3, CH_4, H_2O, $ClONO_2$, CHF_{13}. Expected accuracy: temperature 0.2°, pressure 1% (below 60 km), O_3 profile error 3% if no error in calibration (if 10% calibration error, then ozone profile error is 10%).

HALOE: Gas filter radiometer sensing sunlight (at 2.43–10.25 μm) occulted by atmospheric limb for pressure, HCl, HF, O_3, NO, CH_4, H_2O (2 km resolution in 10–70 km altitude).

ISAMS: Atmospheric limb IR spectrometer for temperature and gases. Pressure-modulated radiometer 2–16 μ for T, CH_4, CO, H_2O, NO, N_2O, O_3, NO_2, HNO_3, N_2O_5, in 15–90 km altitude.

MLS: Senses limb emissions at 63, 183 and 204 GHz (15 channels) for H_2O, O_3, ClO, H_2O_2, temperature, tangent pressure, mesospheric wind in one direction and liquid water near tropopause.

The forthcoming sensors for trace gases include the following (satellites are named in parentheses):

MOPITT (EOS-AM): This four-channel correlation scanning spectrometer has 22 km horizontal and 4 km vertical resolution for CO at 10% accuracy. For total methane, the accuracy is 2%. The measured zone is troposphere.

ILAS-II (ADEOS-II): This will provide the vertical distribution of concentration at 1 km vertical resolution,

from 10 to 60 km, only in higher latitudes (N: 56–70°, S: 63–88°), of O_3, HNO_3, CH_4, N_2O, CFC-11, CFC-12, NO_2, $ClONO_2$ and H_2O besides aerosols, pressure and temperature. The basic accuracy is 5% (1% for ozone), but processing error will be superposed on this. This is a grating-cum-prism spectrometer in the visible (0.753–0.784 μ) with focus on CFC monitoring, and infrared (2–13 μ) for other gases. Sun occultation by the earth's limb is observed.

MIPAS (ENVISAT): This measures concentration profiles of many gases/radicals on a global scale by observing the limb emission in the mid-IR (4–15 μ); most of the outputs are expected in the stratosphere (some in the upper troposphere and some in the mesosphere). The basic approach is a Michelson interferometer. The species sensed include O_3, N_2O, NO, NO_2, HNO_3, HNO_4, N_2O_5, $ClONO_2$, CFCs (five types), HOCl, ClO, CH_4, CO, etc. The vertical resolution is 3 km and the horizontal resolution is 30 km × 300 km. The radiometric precision is 1 to 3% and spectral resolution is 0.025 lines/cm.

SCIAMACHY (ENVISAT): This measures various trace gases in the troposphere and stratosphere via nadir and limb (sun/moon occultation) modes, i.e. total column as well as profiles are retrieved. The spectral range is 0.24–2.4 μ, the vertical resolution is 2.4 km and the altitude range is 10–100 km. The output gases include O_3, O_4, CO, N_2O, NO_2, CH_4, H_2O.

TES (EOS CHEM): 3D profiles on a global scale, of nearly all infrared-active species from the surface to the lower stratosphere will be provided. This is the only instrument giving profiles down to the surface, with a vertical resolution of 2.3 km (in 0–30 km) in the limb mode. There is also a down-looking mode with a horizontal resolution 5 × 50 km. The gases targeted include O_3, CO, CH_4, H_2O, NO and variants, etc.

HIRDLS (EOS-CHEM): This observes the global distribution of the concentration of O_3, H_2O, CH_4, N_2O, NO_2, HNO_3, N_2O_5, CFC-11 and 12, $ClONO_2$, besides aerosols, temperature and polar stratospheric clouds, from the upper troposphere to the mesosphere, at 1 km vertical resolution using IR limb radiometry from 6 to 18 μ. Standard grids over the globe will be employed for data generation at 4° × 4° latitude/longitude, but the basic averaging volume of each data sample will be 1 km × 10 km × 400 km. Trace gases and ozone will be measured at 10% accuracy.

MLS-2 (EOS-CHEM): This measures the lower-stratospheric concentrations of O_3, H_2O, ClO, HCl, OH radical, NO_2, HNO_3 and SO_2 (the last is not a greenhouse gas, but it has the opposite effect of reducing downward radiation by the formation of H_2SO_4 crystals). The limb emission at 215, 310, 640 and 2500 GHz is sensed at 2–4 km vertical bins.

SAGE-III (EOS-AERO/CHEM): This provides profiles of NO_2, OClO with 5–10% accuracy (and ozone at 6%).

GOME-2 (METOP): This is focused on ozone, but also gives ClO, BrO_2, $ClONO_2$, NO and NO_2 profiles at 5 km vertical/160 km horizontal resolution with 10–20% accuracy. It works in the spectral range 0.24–0.79 μ.

IASI (METOP): This measures only the column integrated contents of O_3, CO, CH_4, N_2O and a few other trace gases, at 10% accuracy. It works in the spectral range 3.4–15.5 μ.

Land

Albedo and reflectance: Albedo refers to broadband (entire shortwave) reflected energy, whereas the term reflectance is used at different wavelengths. What is intrinsic to a surface is bi-directional reflectance distribution function (BRDF). The present sensors for albedo/reflectance are NOAA–AVHRR, ERS–ATSR and higher resolution (earth resource) sensors. The latter give high data-rate. Intermediate resolution is provided by IRS WiFS.

POLDER (ADEOS-II): Polarization and directionality of the earth's reflectance will be measured in the 0.44–0.91 μ range, with accuracy of 2–3%. This is a push-broom, wide-field, imaging radiometer/polarimeter with along-track multi-angle views. The 114 degree field-of-view is partitioned into 242 × 274 elements of 7 km × 6 km.

MODIS (EOS AM/PM): This measures among other quantities, short-wave radiance with 5% accuracy. Snow/ice covers are measured with 10% accuracy.

MISR (EOS AM): This gives surface albedo with 03% hemispheric accuracy and BRDF with 1% accuracy.

ASTER (EOS-PM): This gives (15 m) high-resolution as well as stereoscopic images of the surface, clouds, volcanic plumes, etc. The absolute accuracy of VNIR/SWIR radiance is 4%. There are 14 channels from 0.5 to 12 μ.

GLI (ADEOS-II): This gives albedo of snow/ice. It is an optical sensor, advanced version of Ocean Colour and Temperature Sensor (OCTS) on-board ADEOS-I, with 22 + 5 + 7 bands in VNIR + SWIR + M/TIR and spatial resolution 1 km (250 m in some VNIR bands).

Vegetation cover and status: At present, NOAA–AVHRR, IRS–WiFS and INSAT–CCD provide vegetation index at 1 km resolution. This is related to dry bio-matter. At higher resolution, earth resource satellites do give details of vegetation/crop, including their health/vigour, but the data rate is high. Among future sensors for continuous vegetation mapping, the following may be listed:

GLI (ADEOS-II): This has 34 bands from the visible to thermal IR, the focus being on the reflected solar radiation – mainly for ocean colour/chlorophyll. However, even on land, vegetation, snow/ice will be sensed at 250 m spatial resolution. The derived quantities include albedo, vegetation-biomass distribution, etc.

AATSR (ENVISAT-I): Although mainly meant for SST observation, this sensor will also give vegetation

properties such as biomass, moisture, health, growth-stage, etc. Global vegetation index will be derived using two-angle-view.

MERIS (ENVISAT-1): This too is primarily meant for the oceans, but secondarily for land and atmosphere. On land it will provide vegetation/biomass, agriculture, forest, vegetation-stress, forest-fire and snow/ice distribution. The basic sensor-resolution is 250 m, but 4×4 pixels will be combined on-board for global recording, i.e. the overall resolution will be 1 km. Absolute and relative readiometric calibration is provided to permit regular updating and thus maintain long-term stability of data.

CCD (INSAT-2E/3A): This has a 1 km resolution and three bands – visible 0.62–0.68 μ, visible-near infrared 0.77–0.86 μ, and short-wave infrared 1.55–1.69 μ – to provide information on albedo, snow, vegetation index and clouds.

SEVIRI (METEOSAT-Second Generation): This provides vegetation mapping at 5 km resolution although it is mainly used for clouds. It has 12 spectral bands from 0.56 to 13.76 μ capable of capturing one full disk (1/3 of globe) every 15 min.

VEGETATION (SPOT-4/5): At 1.15 km resolution with minimal variation in the off-nadir view, this gives data for use in vegetation monitoring, biosphere/geosphere interaction studies and agriculture.

PRISM (ESA and NASA): This gives data to study land-surface processes. It will have four bands from 0.45 to 12 μ with along-track views at +, –30 degrees, and spatial sampling interval 50 m.

MODIS (EOS-AM/PM): This provides data on biological and physical processes on the surface of the earth and in the lower atmosphere. These include vegetation and snow covers, chlorophyll (fluorescence), land surface temperatures such as net primary productivity, leaf area index, intercepted photo-synthetically active radiation, and corrected vegetation index. Absolute radiance accuracy is 5% at the sensor. Also, by deploying three-angle-view, plant type can be attempted to be identified in the 0.8–1 μ band. The spatial resolution is 'moderate' (500 m).

AWiFS (IRS-P6): Advanced version of present IRS–WiFS, with 60 m resolution and 700 km swath; channels Green, Red, Near IR, SWIR. Vegetation index will be an important product.

Soil moisture: This is not an operational product but several microwave sensors are being experimented with[48]. For climate/GBP purpose, large-area soil moisture, at least in five broad categories, can be attempted from sensors such as DMSP/SSM-I, IRS-P4/MSMR, etc. Secondly, in the arid zone the IR temperature change (rise) in the early morning hours, as seen in the geosynchronous image, may be inversely related to thermal inertia and hence to soil moisture.

Ocean/cryosphere

The current missions geared or amenable to oceanic observations include ERS, TOPEX/POSEIDON, DMSP, IRS-P4 (Oceansat-1), and Sea Star, besides the routine SST mapping from polar (NOAA) and geosynchronous satellites (i.e. GOES, METEOSAT, GMS, FY and INSAT). SST from these meteorological satellites, even with split/multiple window approach, yield values to at best 1°C accuracy with continuous buoy match-ups to update coefficients – the global accuracy is in fact 1.5°C. However, with the use of HIRS together with AVHRR, slight improvement in accuracy is achieved; we can take it as 0.75°C in research mode. On-board IR calibration in NOAA–AVHRR-3 helps in this task. The dual-angle approach of Along Track Scanning Radiometer (ATSR) on ERS, yields a better accuracy, around 0.5° for SST. Both NOAA and ERS/ATSR, have cloud-cover limitation. Microwave radiometer – at present only IRS-P4 MSMR – with 6 GHz channel can sense SST even under a cloud, albeit at a lower accuracy of only 1.5°C. A combination of ATSR and MSMR might yield good coverage and accuracy.

For sea-surface-topography (for circulation and sea-level), altimeter with dual frequency to correct for the ionosphere, and a nadir-looking microwave radiometer to correct for tropospheric water vapour, on a well-tracked satellite is called for. Such is the case with TOPEX/POSEIDON and its net accuracy is judged to be 6 cm. However, after data filtering/processing, even a 2 cm rise in the mean sea level during the mid-1997 El-Nino event could be discerned. In relative terms, between the East and West Pacific, a slope of + 1 cm could be seen before the El-Nino, reversing to about –0.5 cm after the El-Nino.

Coming to the cryosphere, the DMSP/SSMI is routinely mapping sea-ice concentration to an accuracy of 12% and the ice-edge to an accuracy of 12 km. Ice-sheet topography changes have been mapped using ice-mode altimeter data even from the earlier generation GEOSAT. Microwave radiometer SMMR on Nimbus over 1978–87 was employed to detect a 2% decrease per decade in arctic ice-cover, as well as to map variations in sea-ice and ice-extent[42]. For land (mountain) glaciers, only high-resolution earth-resource satellite sensors are useful, but overall snow-cover can use medium resolution sensors, e.g. WiFS on IRS. The sensors planned for the future for ocean/cryosphere in the context of global change are listed below (names of satellites in parentheses).

Ocean colour

MERIS (ENVISAT-1): This sensor with an option of two resolutions at 0.25 and 1 km, has programmable wavelengths in 15 channels, the total range 0.39–1.04 μ

is adjustable at 1.25 nm sampling interval. The bandwidth also is programmable from 1.25 to 25 nm. Large-scale maps (swath being 1150 km) of ocean pigment concentration are expected. Individual components such as chlorophyll, yellow substance and suspended sediments can be distinguished.

MODIS (EOS-AM/PM): With 36 fixed bands from 0.4 to 14.5 μ, this is a multipurpose sensor for biophysical processes on land and in the ocean. Chlorophyll is sensed via fluorescence within 50% when surface water concentration of chlorophyll-*a* is 0.5 mg/m^3. Also, ocean-leaving spectral radiance will be measured to 5% accuracy (from 0.415 to 0.653 μ) resulting in chlorophyll accuracy of 35%. The spatial resolution is 'moderate' (0.25–0.5–1 km in different channels) with global two-day coverage at 2300 km swath. Outputs include chlorophyll, primary productivity, organic matter and sediment transport.

OCM (IRS-P4 and future members in IRS): Chlorophyll, sediments, yellow substance etc. can be inferred from this sensor with 8 bands (400–885 nm) at 360 m resolution and 1420 km swath.

GLI (ADEOS-II): It is an optical sensor with 22 + 5 + 7 bands in VNIR + SWIR + M/T-IR at 1 km resolution (some short-wave bands at 0.25 km). It covers chlorophyll, dissolved organic substances in the ocean, and other features on land (vegetation/snow).

Sea surface temperature

AATSR (ENVISAT-1): With three channels in the thermal IR at two angular views, it aims to achieve 0.4°C accuracy of SST over 0.5° × 0.5° lat/long grids with 80% or less cloud-cover. The basic spatial resolution is 1 km. Multi-angle approach to atmospheric correction will be used.

MODIS (EOS-AM/PM): As described, this has 36 channels ranging up to 14.5 μ. The stated aim is to achieve 0.2°C accuracy in SST, having a 1% precision in TIR radiance.

AVHRR-4 (METOP): With 1 km resolution, 2200 km swath, seven spectral bands and on-board visible/IR calibration targets, this next-generation operational sensor (together with HIRS-4) should provide better SST than present-day AVHRR-3. The visible calibration is an added feature above AVHRR-3, which may provide better thresholding of clouds and sun-glint, thereby increasing the coverage and reliability (though not the accuracy) of SST.

Sea level/topography/inferred-circulation: The sensor for this purpose is the altimeter with local supplement (on circulation) from SAR.

S.S. ALTIMETER (JASON, follow-on to TOPEX/POSEIDON): The solid-state altimeter in C, Ku bands is expected to provide 4 cm precision in sea-level (besides significant wave height to 0.5 m, sea-surface wind speed to 2 m/s). From the global-warming/sea-level-rise point of view, a stable, long-term dataset is planned, to enable detection of a few mm/year trend in mean sea-level.

Sea-ice and ice-sheet (cover/concentration, edge, thickness)

AMSR (EOS-PM, ADEOS-II): This advanced microwave scanning radiometer with eight bands from 6.9 to 89 GHz is meant for atmospheric water in various forms as well as sea-ice mapping. The spatial resolution is 50 km at lower frequencies, ranging to 5 km at 89 GHz.

ASCAT (METOP): Advanced scatterometer at C-band with resolution 50 km, will give sea-ice cover with 10% accuracy, sea-ice-types in four broad classes, and sea-ice-concentration in the footprint.

RA (ESA): Ice-sheet elevation to a few cm accuracy; yet long record can show trend (as in GEOSAT). Horizontal resolution being few km, useful only on flat sheets.

GLAS (EOS LAM): This gives ice elevation to 20 cm at a high (75 m) horizontal resolution (futuristic).

SAR (various satellites): Data over polar regions, received via mobile ground stations, can give the ice-extent (i.e. ice-edge) besides its drift and nature – mainly used for polar ocean navigation, but also can be used in climate study. Data rate being high, is a limitation. Stereo-viewing SAR (as on ERS) can also give detailed ice-topography. SAR works on the principle of recording phase (besides intensity) of returns and employs the Doppler effect due to platform motion to sub-bin the scene.

AVHRR, ATSR (NOAA, ERS): Provides ice-cover and type in cloud-free areas.

Snow-cover on land (and edge, depth)

Nearly all visible/IR/microwave radiometers can map snow-cover, especially where SWIR (1.6 μ) channel is present, to distinguish clouds.

Snow depth may be inferred (only) from snow liquid-water content, amenable to microwave remote sensing, e.g. from AMSR on ADEOS-II, and by ASCAT on METOP.

Concluding remarks

Table 3 summarizes the comparison of desired vs achievable accuracies of some important parameters. An earlier review by the present authors[49] may also be seen.

The space agencies of all the active nations are well-cognisant of the need for an intensive, coordinated, and

Table 3. Global change parameter accuracies

		Required/desirable[@]				Achieved/expected		
Sl. no.	Parameter	Accuracy	Horizontal resolution (km)	Vertical resolution (km)	Sensor/satellite	Accuracy (same units)	Horizontal resolution (km)	Vertical resolution (km)
1	Temperature profile	0.5 K	250	2	ATOVS/NOAA-K-N	1.5	40	2
					AIRS/EOS-PM-1	1.0	25	2
					IMG/ADEOS-2	1.0	100	2
					IASI/METOP-1	1.0	25	2
2A	Humidity profile (1000–500 mb)	0.5 g/kg	250	2	AMSU-B/NOAA-K-M	0.75	20	1
					AIRS/EOS-PM-1	0.5	25	1
					IASI/METOP-1	0.5	25	1
					SAPHIR/Megha Trop.	0.75	10	2
2B	Humidity profile (500–100 mb)	0.05 g/kg	250	2	AIRS/EOS-PM-1	0.05	25	1
					IASI/METOP-1	0.05	25	1
					MHS/METOP & EOS	0.08	50	1
					SAPHIR/Megha Trop.	0.08	10	2
3A	Ozone column	20 DU	100	N/Ap	AIRS/EOS-PM-1	20(10%)	25	N/Ap
					IASI/METOP-1	20(10%)	25	N/Ap
					SCIAMACHY/ENVISAT	1%	30 × 200	N/Ap
					GOMOS/ENVISAT	0.5%	N/Av	N/Ap
3B	Ozone profile	5%	250	2	GOME-2/METOP-1	15%	160	5
					SCIAMACHY/ENVISAT	RP*4%	30 × 200	2.5
					MIPAS/ENVISAT	RP*1%	30 × 200	2.5
					HIRDLS/EOS-CHEM	10%	10 × 400	1
					TES/EOS-CHEM	20 ppbv	50	2.5
					ILAS-2/ADEOS-2	5%	13	1
					SAGE-III/EOS-AERO	6%	N/Av	2
					GOMOS/ENVISAT	5%	N/Av	1
4	Other trace gas profiles	5%	250	2	MOPITT/EOS-AM	2%	22	4
					TES/EOS-CHEM	N/Av	50	2.5
					ILAS-2/ADEOS-2	15%	22	1
					MIPAS/ENVISAT	RP*3%	30 × 300	3
					SCIAMACHY/ENVISAT	RP*4%	30 × 200	2.5
5	Aerosol load	10%	250	2	GOMOS/ENVISAT	10%	N/Av	1
					SAGE-III/EOS-AERO	10%	N/Av	2
					MISR/EOS-AM	10%	15	Total
					MODIS/EOS-AM	10%	1	Total
					SCIAMACHY/ENVISAT	RP*4%	30 × 200	2.5
6	Vegetation index	5% Irrad.	50	N/Ap	MODIS/EOS-AM	5%	1	N/Ap
					CCD/INSAT-3A	5%	1	N/Ap
					AWiFS/IRS-P6	5%	0.06	N/Ap
7	SST	0.25K	250	N/Ap	AATSR/ENVISAT	0.4K	50	N/Ap
					MODIS/EOS-AM	0.2K	1	N/Ap
					AVHRR-4/METOP	0.5K	100	N/Ap
8	Sea topography	5 cm	250	N/Ap	S.S.ALT/JASON	4	250	N/Ap
					ALT/EOS-PM	5	25	N/Ap
9	Sea-ice-cover	10%	100	N/Ap	ASCAT/METOP	10%	50	N/Ap

N/Ap, Not applicable; N/Av, Not available; [@]Requirements mainly taken from WMO (ref. 50).
*Radiometric precision is mentioned. Gas profile accuracy will depend on inversion.

Appendix

			Category: Satellite/Sensor
1.	AATSR	Advanced Along Track Scanning Radiometer	Sen.
2.	ADEOS	Advanced Earth Observation Satellite	Sat.
3.	AEM	Atmospheric Explorer Mission	Sat.
4.	AIRS	Atmospheric Interferometric Radiometric Sounder	Sen.
5.	ALT	Altimeter	Sen.
6.	AMSR	Advanced Microwave Scanning Radiometer	Sen.
7.	AMSU	Advanced Microwave Sounding Unit	Sen.
8.	ASCAT	Advanced Scatterometer	Sen.
9.	ASTER	Advanced Spaceborne Thermal Emission and Reflection Radiometer	Sen.
10.	ATLID	Atmospheric LIDAR	Sen.
11.	ATOVS	Advanced TIROS Operational Vertical Sounder	Sen.
12.	ATSR	Along Track Scanning Radiometer	Sen.
13.	AVHRR	Advanced Very High Resolution Radiometer	Sen.
14.	AWIFS	Advanced Wide Field Sensor	Sen.
15.	CCD	Charge-Coupled Device	Sen.
16.	CERES	Cloud and Earth's Radiant Energy System	Sen.
17.	DMSP	Defense Meteorological Satellite Programme	Sat.
18.	EOS	Earth Observation Satellite	Sat.
19.	EOSP	Earth Observing Scanning Polarimeter	Sen.
20.	ERBE	Earth Radiator Budget Experiment	Sen.
21.	ERBSAT	Earth Radiation Budget Satellite	Sat.
22.	ERS	European Remote Sensing Satellite	Sat.
23.	GLAS	Geoscience Laser Altimeter System	Sen.
24.	GLI	Global Imager	Sen.
25.	GMS	Geosynchronous Meteorological Satellite	Sat.
26.	GEOS	Geosynchronous Operational Environmental Satellite	Sat.
27.	GOME	Global Ozone Monitoring Experiment	Sen.
28.	GOMOS	Global Ozone Monitoring by Occultation of Stars	Sen.
29.	HIRDLS	High Resolution Dynamic Limb Sounder	Sen.
30.	HIRS	High Resolution Infrared Sounder	Sen.
31.	IASI	Infrared Atmospheric Sounding Interferometer	Sen.
32.	ILAS	Improved Limb Atmospheric Spectrometer	Sen.
33.	IMG	Interferometric Monitoring of Gases	Sen.
34.	INSAT	Indian National Satellite	Sat.
35.	IRS	Indian Remote Sensing Satellite	Sat.
36.	MADRAS	Microwave Analysis & Detection of Rain & Atmospheric Structure	Sen.
37.	MERIS	Medium Resolution Imaging Spectrometer	Sen.
38.	METOP	Operational Meteorology Satellite	Sat.
39.	MHS	Microwave Humidity Sensors	Sen.
40.	MIPAS	Michelson Interferometer for Passive Atmospheric Sounding	Sen.
41.	MISR	Multi-angle Imaging Spectro-Radiometer	Sen.
42.	MODIS	Moderate-Resolution Imaging Spectrometer	Sen.
43.	MOPITT	Measurement of Pollution in the Troposphere	Sen.
44.	MOS	Multispectral Opto-electronic Scanner	Sen.
45.	MSMR	Multichannel Scanning Microwave Radiometer	Sen.
46.	MSU	Microwave Sounding Unit	Sen.
47.	NOAA	National Oceanic & Atmospheric Administration	Sat.
48.	OCM	Ocean Colour Monitor	Sen.
49.	POLDER	Polarisation and Directionality of the Earth's Reflectance	Sen.
50.	PRISM	Process Research by Imaging Space Mission	Sat.
51.	RA	Radar Altimeter	Sen.
52.	SAFIRE	Spectroscopy of the Atmosphere using Far. Infrared Emission	Sen.
53.	SAGE	Stratospheric Aerosol and Gas Experiment	Sen.
54.	SAMS	Stratospheric and Mesospheric Sounder	Sen.
55.	SAPHIR	Sondeur Atmospherique du Profil d'Humidite Intertropicale par Radiometrie	Sen.
56.	SAR	Synthetic Aperture Radar	Sen.
57.	SBUV	Solar Backscatter Ultra-Violet	Sen.
58.	Sca Ra B	Scanner for Radiation Budget	Sen.
59.	SCIAMACHY	Scanning Imaging Absorption Spectrometer for Atmospheric Chartography	Sen.
60.	SEVIRI	Spinning Enhanced Visible & InfraRed Imager	Sen.
61.	SMMR	Scanning Multifrequency Microwave Radiometer	Sen.
62.	SSALT	Solid State Altimeter	Sen.
63.	SSM/I	Special Sensor Microwave, Imager	Sen.
64.	SSU	Stratospheric Sounding Unit	Sen.
65.	TES	Tropospheric Emission Sensor	Sen.
66.	TIROS	Television InfraRed Operational Satellite	Sat.
67.	TOMS	Total Ozone Mapping Spectrometer	Sen.
68.	TOPEX	Ocean Topography Experiment	Sat.
69.	TOVS	Tiros Operational Vertical Sounder	Sen.
70.	TRMM	Tropical Rainfall Measuring Mission	Sat.
71.	UARS	Upper Atmospheric Research Satellite	Sat.
72.	VHRR	Very High Resolution Radiometer	Sen.
73.	VTPR	Vertical Temperature Profile Radiometer	Sen.
74.	WiFS	Wide Field Sensor	Sen.

long-drawn programme of observation of the globe from the point of view of geosphere–biosphere interactions and changes. The Committee on Earth Observation Satellites has already incorporated this requirement among the many that will be addressed by the planned satellites. The sensors, most of them with a considerable heritage (and a few somewhat futuristic ones, calling for fuller test and validation), are already either in place or on the anvil. The inter-calibration of different and successive sensors, and standardization of the data-processing algorithms are critical elements in the total plan so as to maintain accuracy and consistency of data. A few parameters require further sensor development to achieve the desired observability, e.g. ocean salinity[48], near-surface air temperature, surface pressure, etc.

1. Kondratyev, K. Y. and Cracknell, A. P., *Observing Climate Change*, Taylor & Francis, 1998, p. 562.
2. NASA, From Pattern to Process: The Strategy of the Earth Observing System, EOS Science Steering Committee Report vol. II, 1987, p. 140.
3. Gorshkov, V. G., *Physical and Biological Bases of Life Stability, Man, Biota, Environment*, Springer-Verlag, Berlin, 1995.
4. Waring, R. H. *et al.*, *Oceanologia*, 1985, **66**, 127–137.
5. Seller, P. J., Biophysical models of land surface processes. In *Climate System Modeling* (ed. Trenberth, K. E.), Cambridge Univ. Press, 1992, chap. 14, pp. 451–490.
6. Arrhenius, S., *Philos. Mag.*, 1896, **41**, 237–275.
7. Revelle, R. and Suess, H. E., *Tellus*, 1957, **9**, 18–27.
8. Cellendar, G. S., *Q. J. Roy. Meteorol. Soc.*, 1938, **64**, 223–227.
9. Sud, Y. C., Shukla, J. and Mintz, Y., *J. Appl. Meterol.*, 1988, **27**, 1036–1054.
10. Ramanathan, V. *et al.*, *Rev. Geophys.*, 1987, **25**, 1441–1482.
11. Houghton, J. T., Jenkins, G. J. and Ephraums, J. J. (eds), Climate Change, The IPCC Scientific Assessment Report, Intergovernmental Panel on Climate Change, Cambridge University Press, 1990, p. 362.
12. Houghton, J. T., Taylor, F. W. and Rodgers, C. D., *Remote Sounding of Atmospheres*, Cambridge University Press, Cambridge, 1984.
13. Kaplan, L. D., *J. Opt. Soc. Am.*, 1959, **49**, 1004.
14. Houghton, J. T., *Q. J. R. Meteorol. Soc.*, 1969, **95**, 1–20.
15. Rodgers, C. D., *Rev. Geophys. Space Phys.*, 1976, **14**, 609–624.
16. Susskind, J., Rosenfield, J. and Reuter, D., *J. Geophys. Res.*, 1983, **88**, 8550–8568.
17. Liou, K. N., *An Introduction to Atmospheric Radiation*, Academic Press, New York, p. 392.
18. Hayden, R. A., Hubert, C. F., McClain, E. P. and Seaman, R. S., Quantative meteorological data from satellites. WMO-TN 166, WMO No. 531, Geneva, 1979, p. 32.
19. Issacs, R. G., Review of 183 GHz moisture profile retrieval studies, AFGL-TR-87-0127, 1987, p. 52.
20. Smith, W. L., Howell, H. B. and Woolf, H. M., *J. Atmos. Sci.*, 1979, **36**, 566–676.
21. Gille, J. C. and House, F. B., *J. Atmos. Sci.*, 1971, **29**, 1427–1442.
22. Gille, J. C., Hailey, P. L. and Russel, J. M. III., *Philos. Trans. R. Soc., London Ser A*, 1980, **296**, 205–218.
23. Drummond, J. R., Houghton, J. T., Peskett, G. D., Rodgers, C. D., M. J., Whitney, J. and Williamson, E. J., *Philos. Trans. R. Soc., London Ser A*, 1980, **296**, 219–241.
24. Rawcliffe, R. D. and Elliot, D. D., *J. Geosphys. Res.*, 1966, **71**, 5077–5089.
25. Anderson, G. P., Barth, C. A., Cayla, F. and London, J., *Ann. Geophys.*, 1969, **25**, 239–243.
26. Frederick, J. E., Hays, P. B., Guenther, B. W. and Heath, D. F., *J. Atmos. Sci.*, 1977, **34**, 1987–1994.
27. Heath, D. F., Krueger, A. J., Roeder, H. A. and Henderson, B. D., *Opt. Eng.*, 1975, **14**, 323–331.
28. Riegler, G. R., Drake, J. F., Liu, S. C. and Circerone, R. J., *J. Geophys. Res.*, 1976, **81**, 4997–5002.
29. Hays, P. B. and Roble, R. G., *J. Atmos. Sci.*, 1968, **25**, 1141–1153.
30. Gunson, M. R., Farmer, C. B., Norton, R. H., Zander, R., Rinsland, C. P., Shaw, J. H. and Gao, B. C., *J. Geophys. Res. D*, 1990, **95**, 13867–13882.
31. Wark, D. Q., Hilleary, D. T., Anderson, S. P. and Fischer, J. C., *IEEE Trans. Geosci. Electron*, 1970, **GE-8**, 264–270.
32. Goede, A. P. H. *et al.*, *Adv. Space Res.*, 1991, **11**, 243–246.
33. Hanel, R. A. *et al.*, *Climatic Change*, 1995, **31**, 247–271.
34. Abel, P. J. *et al.*, *Proc. R. Soc., London Ser. A*, 1970, **320**, 35–55.
35. Curtis, P. O., Houghton, J. T., Peskett, G. D. and Rodgers, C. D., *Proc. R. Soc., London Ser A*, 1974, **337**, 135–150.
36. Taylor, F. W. *et al.*, *J. Geophys. Res. D*, 1993, **98**, 10799–10814.
37. Michael, Janssen, A. (ed.), *Atmospheric Remote Sensing by Microwave Radiometry*, John Wiley & Sons, 1993.
38. Kramer, H. J., *Observation of the Earth and its Environment, Survey of Missions and Sensors*, Springer-Verlag, Berlin, 1994, 2nd edn, p. 580.
39. Smith, W. L., *Adv. Space Res.*, 1989, **9**, 363–372.
40. Waters, J. W. *et al.*, *Nature*, 1993, **362**, 597–602.
41. Joseph, George, *Remote Sensing Rev.*, 1996, **13**, 257–342.
42. Gloersen, P. and Campbell, W. J., *J. Geophys. Res.*, 1988, **93**, 10666–10674.
43. Haeberli, W., *Ann. Glac.*, 1990, **14**, 99–101.
44. Gruber, A. and Jacobowitz, H., *Adv. Space Res.*, 1985, **5**, 111–120.
45. Robinson, D. A., Dewey, K. F. and Heim, R. R. Jr., *Bull. Am. Meterol. Soc.*, 1993, **74**, 1689–1696.
46. Jones, P. D. *et al.*, *J. Geophys. Res.*, 2001, **106**, 3371–3380; as adapted in *Climate Change*, IPCC Assessment Report (The Scientific Basis), co-ordinating lead authors Folland, C. K. and Karl, T. R., 2001, chapter 2, p. 121.
47. Hansen, J. *et al.*, *Climatic Change*, 1995, **31**, 247–271.
48. Martin-Neira, M. and Goutule, J. M., *ESA Bull.*, 1997, **92**, 95–104.
49. Desai, P. S. and Joseph, George, *Indian J. Radio Space Phys.*, 1994, **23**, 101–124.
50. World Meteorological Organization, Preliminary statement of guidance regarding how well satellite capabilities meet WMO user requirements in several application areas, WMO Tech. Doc., 1998, vol. 913, p. 66.

ACKNOWLEDGEMENTS. We thank Prof. B. H. Subbaraya and Dr V. Jayaraman, Indian Space Research Organization, for reviewing the manuscript and offering valuable comments. Several colleagues have given useful inputs.

Received 7 March 2001; revised accepted 21 June 2003